Experimental and computational equilibria of fieldreversed configurations

R. L. Spencer and M. Tuszewski

Citation: Physics of Fluids (1958-1988) **28**, 1810 (1985); doi: 10.1063/1.864924
View online: http://dx.doi.org/10.1063/1.864924
View Table of Contents: http://scitation.aip.org/content/aip/journal/pof1/28/6?ver=pdfcov
Published by the AIP Publishing

Experimental and computational equilibria of field-reversed configurations

R. L. Spencer and M. Tuszewski
Los Alamos National Laboratory, University of California, Los Alamos, New Mexico 87545

(Received 22 August 1984; accepted 6 February 1985)

Experimental measurements on the field-reversed configurations produced in the FRX-C device [Plasma Phys. **26**, 991 (1984)]are compared to corresponding measurements on numerically computed magnetohydrodynamic equilibria. Good agreement between experiment and theory is obtained for magnetohydrodynamic (MHD) equilibria with separatrix betas of about 0.6. The experimental measurements indicate that the separatrix is more elliptical and that the flux surfaces are distributed more gently in the axial direction than in the equilibria computed previously. A sharp spike in $dp/d\psi$ at the separatrix is found to produce computed equilibria similar to those observed experimentally. The effect of end mirrors and toroidal field on equilibrium properties is also discussed.

I. INTRODUCTION

A field-reversed configuration (FRC) is an elongated compact toroid that is formed without toroidal field.[1] After formation, these plasmas are observed to be in grossly stable equilibrium for many Alfvén transit times. Detailed information about these elongated equilibria is required for stability and transport studies. Early experimental data[1] suggested that the flux surfaces in these objects are not elliptical but are rather more racetracklike in shape. This is consistent with two-dimensional computations[2,3] of FRC equilibria bounded by an infinitely long conducting cylinder. Recent experimental work on the FRX-C device[4] showed that the FRC separatrix is almost elliptical, but no conclusion was drawn about the shape of the internal flux surfaces. To extract further information from these data, numerically computed FRC equilibria were produced in the coil geometry of the FRX-C device. A diagnostic code was used to compare this numerical work with the available experimental data. This comparison confirms some previously inferred equilibrium features,[4] shows the influence of the passive end mirrors and toroidal field on the equilibria, and yields some qualitative information about the distribution of flux surfaces inside the separatrix. In particular, it is found that the experimentally observed equilibria have a more gentle axial distribution of inner flux surfaces than those computed previously.[2,3] Magnetohydrodynamic (MHD) equilibria having this property can be computed by making the pressure profile quite steep as a function of flux near the separatrix. In Sec. II, we describe the experiment and the equilibrium calculation. In Sec. III, a comparison between experimental data and numerical results is presented, and in Sec. IV conclusions are given. In Appendix A, the change in the average beta condition produced by end mirrors is discussed. In Appendix B, the effect of toroidal field on the average beta condition and on the axial distribution of flux surfaces is discussed.

II. DESCRIPTION OF THE EXPERIMENT AND OF THE EQUILIBRIUM CALCULATION

The FRX-C device is a field-reversed theta pinch with a coil of length 2 m and of radius $r_w = 25$ cm. A description of this experiment, of its diagnostics, and of the FRC formation method can be found elsewhere.[5] At each end of the coil is a passive mirror of about 20 cm axial extent and of radius $r_m = 22$ cm to provide for symmetrical FRC formation and for axial positioning. Figure 1 is to scale and shows the coil geometry for a half-system (the coil is symmetric about the $z = 0$ plane). The most complete experimental data were obtained at a fill pressure of 20 mTorr[4] and with l (the FRC half-length) comparable to z_m (the axial location of the end mirror step). In this paper, we restrict ourselves to data taken at this fill pressure where $n \simeq 5 \times 10^{15}$ cm^{-3} and $T_e \simeq T_i \simeq 100$ eV. The equilibrium features of these plasmas were diagnosed experimentally with an excluded-flux array and with two side-on interferometers. The first diagnostic yields the excluded flux profile, $r_{\Delta\phi}(z)$; it approximates the shape of the separatrix, $r_s(z)$.[1,6] The quantity $r_{\Delta\phi}(z)$ is defined by $r_{\Delta\phi}(z) = r_w(1 - \psi_p B_v/\psi_v B_p)^{1/2}$, where ψ_p and B_p are the flux and the magnetic field, respectively, at the coil with an FRC present, and where ψ_v and B_v are the flux and the magnetic field, respectively, at the coil with no FRC present. One side-on interferometer measures $\int n\, dr$ along a chord that is radially and axially variable, while the other measures $\int n\, dr(0)$ along a diameter at $z = 0$ to allow discharge to discharge variations to be taken into account. The excluded flux array does not yield any information about the flux surfaces inside the separatrix, but the various interferometric scans do (assuming that the temperature is constant inside the separatrix), and this information was extracted by comparing the experimental results with data obtained by analyzing numerically computed two-dimensional equilibria.

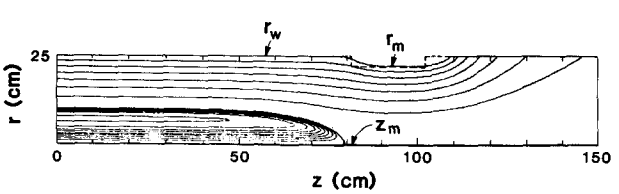

FIG. 1. A typical FRC equilibrium in the FRX-C coil geometry is displayed. The outer rectangular frame is the computational area. The actual end mirror geometry is indicated with dotted lines. This equilibrium has $\beta_s = 0.6$ and equilibrium parameters $a = 73.18$, $b = 98.16$, $c = 167.6$, $e = 0.0$, $g = 0.0$, and $I_\theta = 13.9$. In the computation there were 102 radial mesh points and 153 axial mesh points.

 0031-9171/85/061810-06$01.90

Equilibria were computed by using a code written by Hewett; details are found in Ref. 3. The boundary conditions in the code were altered to model the FRX-C experiment by changing the value of the poloidal flux function, ψ, along the outside of the region shown in Fig. 1. To model the passive end mirror, $|\psi|$ was increased in the vicinity of the mirror step in such a way that the correct mirror ratio was obtained at $r=0$ below the mirror and so that the mirror length was approximately correct. The discrepancy between the approximation and the actual passive mirror is indicated in Fig. 1. To model the end of the coil, the values of ψ at $r=25$ cm, $z>100$ cm, and at $z=150$ cm were fixed at the values they would have for a finite length coil without an FRC present. Reflection boundary conditions were used at $z=0$, $\psi=0$ at $r=0$, and $\psi=-1$ at $r=r_w$. The Grad–Shafranov equation was solved with these boundary conditions in the region indicated in Fig. 1 with a profile of $dp/d\psi$ given by

$$\frac{dp}{d\psi}=c\left\{\frac{e}{1+g\psi^2}+\begin{bmatrix}1+a\psi, & \psi>0\\ \exp(b\psi), & \psi\leqslant 0\end{bmatrix}\right\}, \tag{1}$$

where a, b, c, e, and g are constants. Note that in Eq. (1), we have $\psi>0$ inside the separatrix and $\psi\leqslant 0$ outside the separatrix, so that the pressure cuts off on open field lines for positive b and large g. To obtain equilibria in the geometry of Fig. 1, it was found necessary to cut off $dp/d\psi$ as a function of z for $z>l$. Otherwise, after a few iterations the FRC would set up in the low field region beyond the mirror on the far right in Fig. 1. The characteristic length for the cutoff was the wall radius, so at $z=90$ cm, the largest value of z for which theory and experiment are compared, the pressure was not affected very much (15%). The one-dimensional code described in Ref. 3 was used to find values of the constants that gave fixed values of $x_s=r_s/r_w$ and β_s, the ratio of the separatrix pressure to the peak pressure; it was also used to adjust the amount of pressure profile gradient at the separatrix (controlled by the constants e and g). Once the constants were determined, the resulting pressure profile was employed in the two-dimensional equilibrium code to produce an equilibrium for comparison with the experiments. As described in Ref. 3, the total current I_θ was adjusted to obtain an equilibrium of the desired length. Once the equilibrium was successfully computed, the same diagnostics used in the experiments were applied to it, albeit in FORTRAN form. Equilibrium data and corresponding data from a calculation with no plasma present were used to obtain the excluded flux $r_{\Delta\phi}(z)$; interferometry scans were performed by assuming that the temperature is constant so that density and pressure are directly proportional everywhere. Experimental measurements[1,7] and calculations[8] indicate that the isothermal assumption is approximately valid inside the separatrix. Outside the separatrix the temperature falls off quite rapidly, which causes the density to be underestimated there by the diagnostic code.

One important feature of FRC equilibria that is not included in these calculations is rotation. An $m=2$ rotational instability[1,9] develops at the end of the FRC equilibrium phase when the plasma rotational frequency reaches an appreciable fraction of the diagmagnetic drift frequency Ω^*. For the 20 mTorr data[4] analyzed here, $\Omega^*\simeq 2\times 10^5$ Hz. The magnitude of the equilibrium change caused by rotation can be estimated by comparing[10] the centrifugal pressure $P_c=m_i\int\omega^2 r\,dr$ with the plasma pressure $P_K=n(T_e+T_i)$. For the data analyzed here, assuming $\omega=0.5\Omega^*$, the ratio of these pressures is $P_c/P_K=0.03$, so that the contribution of rotation to the equilibrium is quite small. Therefore, plasma rotation is not included in the computation of FRC equilibria in this paper. However, it should be recognized that the contribution of rotation to FRC equilibrium may be substantial at low fill pressures and for smaller sized devices.[9]

III. COMPARISON OF EXPERIMENTAL AND COMPUTATIONAL RESULTS

At 20 mTorr fill pressure, and at $z=0$, the FRC's have values for $r_{\Delta\phi}\simeq r_s$ of about 10 cm, corresponding to $x_s=0.4$. The open circles in Fig. 2 show the values of $r_{\Delta\phi}/r_{\Delta\phi}(0)$ obtained from the excluded flux array at several locations in z (the data points in this paper are averages over 5 to 20 discharges, and the error bars are standard deviations). To fit these data, several equilibria were computed. All were required to give the correct value of $r_{\Delta\phi}$ in the midplane and to fit the variation of $r_{\Delta\phi}(z)$ as well as possible. The variation of $r_{\Delta\phi}$ with length for computed equilibria with $\beta_s=0.5$, 0.6, and 0.7 is shown by the solid lines in Fig. 2. For all three of these equilibria $e=g=0$. We observe from this figure that good agreement between computed and experimental data is obtained for β_s in the range 0.6 to 0.7. The best least-square fit to the experimental data is obtained for $\beta_s=0.6$. For $\beta_s=0.5$, the computed profiles are too racetracklike around $z=50$ cm, and this effect is even more pronounced at values of β_s less than 0.5.

The computed equilibria used in making Fig. 2 all have $l\simeq z_m\simeq 80$ cm; the one with $\beta=0.6$ is shown in Fig. 1. All three of the cases used in Fig. 2 have a value of $\langle\beta\rangle\simeq 0.95$, where $\langle\beta\rangle$ is the average over the area inside the separatrix at $z=0$ of the ratio of the pressure to the peak pressure (at the field null). This value of $\langle\beta\rangle$ is greater than the commonly used value of $\langle\beta\rangle=1-x_s^2/2=0.92$ predicted for a FRC in a cylindrical flux conserver. Since kinetic effects are not included in the equilibrium calculation, this change must be due either to plasma on open field lines or to the mirror. The effect of plasma on open field lines can be computed from Eq.

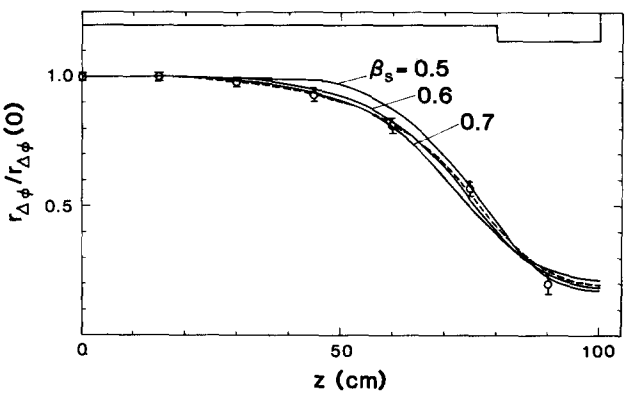

FIG. 2. Normalized excluded flux radius profiles as functions of z are displayed. The experimental data are given with open circles and the results of computations are given with solid and dotted lines.

(A10) of Ref. 3; it is found to decrease $\langle\beta\rangle$, but by less than 1%. Hence, the increase in the average beta must be due to the mirrors. In Appendix A the effect of the mirrors is estimated and a formula is found that agrees well with the computed results. The increase in the average beta caused by the mirrors is significant because a FRC with $\langle\beta\rangle = 1$ would be completely unmagnetized and have $\beta_s = 1$, implying increased kinetic effects and transport. As an example, a particle transport model[11] is used to calculate the particle confinement time τ_N and the parameter $\bar{s} = \int_0^R r\,dr/r_s\rho_i$, which measures FRC magnetization and stability,[12] for values of $\langle\beta\rangle$ of 0.92 and 0.95. The results of this calculation are shown in Table I. Also included in this table are the values of β_s (the calculation assumes an isothermal plasma) and of the characteristic width w of the open-field-line plasma layer (in units of ion gyroradii in the external field). We observe from Table I that the increase in $\langle\beta\rangle$ from 0.92 to 0.95 results in higher values of β and w, in closer agreement with the experimentally inferred values[4] of about 0.6 and 4, respectively. Furthermore, the value of $\tau_N = 177$ μsec is in better agreement with the experimental estimate[13] of 154 μsec for the 20 mTorr data. We also note from Table I that $\bar{s}$ is substantially decreased for $\langle\beta\rangle = 0.95$, which may provide increased stability due to kinetic effects.[14] It is interesting to note that the influence of the end mirrors on $\langle\beta\rangle$ decreases as x_s increases, as discussed in Appendix A.

The three computed equilibria with values of β_s of 0.5, 0.6, and 0.7 that were used in Fig. 2 have been analyzed with the diagnostic code for comparison with the experimental interferometry data. The computed and experimental values of $\int n\,dr/\int n\,dr(0)$, obtained as a function of the impact parameter d of the radially variable chord at (a) $z = 0$ and (b) $z = 90$ cm, are given in Fig. 3 with solid curves and circles, respectively. We observe from Fig. 3(a) that at $z = 0$ and at small values of d, there is good agreement between the computed equilibrium with $\beta_s = 0.6$ and the experimental data. However, for values of $d \geqslant 5$ cm, the computed curves lie below the experimental data, reflecting a smaller amount of plasma on open field lines in the computation ($w \simeq 2$) than in the experiment ($w \simeq 4$). Since lower plasma temperatures are expected outside the separatrix,[7,8] the assumption in the computed curves of constant temperature everywhere underestimates the density outside the separatrix; this could account for part of the discrepancy. This observation also applies to the comparison between computed and experimental data at $z = 90$ cm in Fig. 3(b), and suggests a closer agreement between the computed curve for $\beta_s = 0.6$ and the experimental data.

The computed and experimental vlaues of $\int n\,dr/\int n\,dr(0)$ taken on diameters ($d = 0$) as a function of z are given in Fig. 4; the three solid curves are for the previously

TABLE I. Calculated dependence of the FRC confinement and stability on $\langle\beta\rangle$.

$\langle\beta\rangle$	β_s	w	τ_N (μsec)	$\bar{s}$
0.92	0.47	1.8	211	2.3
0.95	0.56	1.6	177	1.6

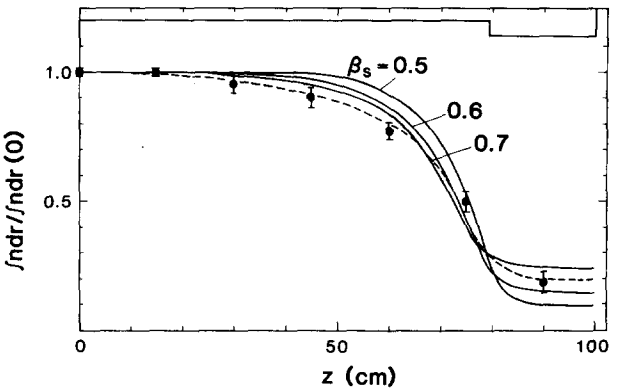

FIG. 3. Normalized interferometry profiles as functions of z are displayed. The experimental data are given with solid circles and the results of computations are given with solid and dotted lines.

mentioned computed equilibria. We observe from Fig. 4 that all of the computed curves lie above the experimental data points for values of z in the range 30 to 60 cm. This suggests that the computed equilibria are more racetracklike in shape than the experimental equilibria. This observation is not influenced by the amount of plasma on open field lines since $\int n\,dr$ has been shown[4] to be insensitive to this effect for $d = 0$, for then the path length through the interior plasma greatly exceeds the width of the open-field-line layer. The computed curves of $\int n\,dr/\int n\,dr(0)$ are nearly identical to those of $r_{\Delta\phi}/r_{\Delta\phi}(0)$ for $z \leqslant 60$ cm, reflecting the nearly one-dimensional nature of the computed equilibria over their central portion. This can easily be seen in the inner flux surface distribution shown in Fig. 1.

To compute equilibria that have the more gentle axial distribution of flux surfaces indicated by the experimental data, the function $p(\psi)$ must be appropriately chosen. (Note: since it appears that equilibria with a rather uniform axial distribution of flux surfaces also have elliptical separatrices, such equilibria will be referred to as "elliptical equilibria" in

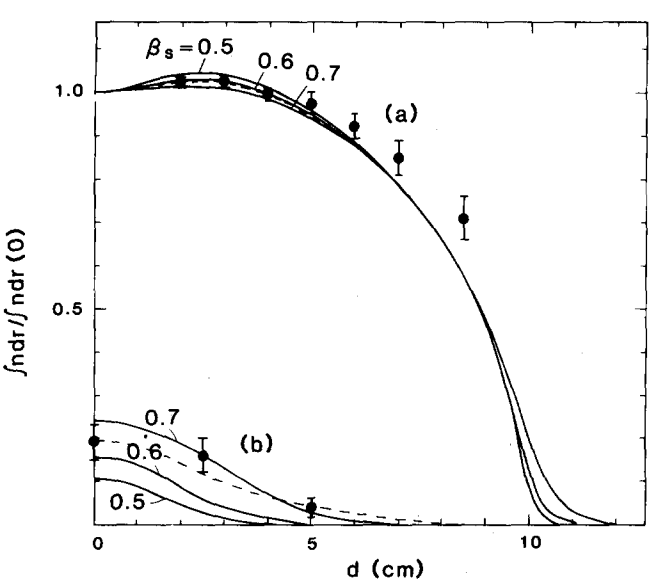

FIG. 4. Normalized interferometry profiles as functions of the impact parameter d are displayed for (a) $z = 0$ cm and for (b) $z = 90$ cm. The experimental data are given with solid circles and the computations are given with solid and dotted lines.

the following discussion.) An obvious thing to try is to make $p(\psi)$ be more peaked at the magnetic axis, but the axial distribution of flux surfaces is hardly affected by this change. The way to make the equilibria more elliptical can be discovered in the equilibrium calculations of Shumaker[15] and of Grossmann and Saltzmann.[16] In these calculations the entropy function $Q_p(\psi) = p(\psi)[\oint dl/B]^r$ is specified rather than the pressure. In Ref. 16, $Q_p = 0$ at the separatrix, so p and $dp/d\psi$ are both zero there; higher derivatives are, however, singular. In Ref. 17, Q_p has a finite value at the separatrix so that p and $dp/d\psi$ are both singular there. This singularity seems to affect the shape of the equilibrium. In Shumaker's calculation the singularity is handled by setting $dp/d\psi$ to a large but finite value at the separatrix. This is only a very approximate way to handle the actual singularity since the even singularity in p should produce an odd singularity in $dp/d\psi$. Shumaker's procedure treats the singularity in $dp/d\psi$ as if it were even so that p is nonsingular, but has a very steep gradient at the separatrix. The result of this large spike in $dp/d\psi$ at the separatrix is a very elliptical FRC equilibrium, too elliptical, in fact, to match the experimental measurements reported here. In the calculations of Grossmann and Saltzmann, the singularity occurs in higher-order derivatives and the resulting equilibria are not elliptical, but neither are they as flat in the midplane as the equilibrium displayed in Fig. 1. To include this effect in our calculation, we added a Lorentzian centered on the separatrix to $dp/d\psi$, as shown in Eq. (1). The result of adding this spike is shown in Fig. 5. Note that the separatrix is more elliptical and that the flux surfaces are distributed more evenly in the axial direction. Because the spike in $dp/d\psi$ is so sharp, Fig. 5 probably does not represent the precise solution of the Grad–Shafranov equation for the equilibrium parameters chosen, but the qualitative effect of making axial gradients more gentle is probably correct. This discussion only applies, of course, to MHD equilibrium. It is possible that a fully kinetic equilibrium might more naturally produce an equilibrium with the desired shape. This discussion has also neglected the effect of toroidal field. This is treated in Appendix B where it is shown that toroidal field does not produce elliptical equilibria.

The equilibrium of Fig. 5 was analyzed with the diagnostic code and the results of this analysis are indicated by the dotted lines in Figs. 2–4. The main change between this new computation and the former ones is the good agreement obtained in Fig. 3 between experimental and computational profiles of $\int n\, dr/\int n\, dr(0)$ as functions of z. The better agreement comes from a more gradual distribution of inner flux surfaces (seen by comparing the equilibria of Figs. 1 and 5) as well as from a somewhat more elliptical $r_{\Delta\phi}(z)$ profile (seen in Fig. 2).

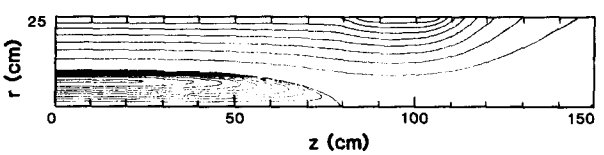

FIG. 5. A more elliptical equilibrium in the FRX-C coil geometry is displayed. The equilibrium parameters are $a = 10.1$, $b = 23.1$, $c = 21.6$, $e = 13.4$, $g = 328000.0$, and $I_\theta = 13.1$. In the computation there were 102 radial mesh points and 153 axial mesh points.

IV. CONCLUSIONS

Experimentally produced FRC's have been compared with MHD equilibrium calculations for the same geometry. By judicious choice of parameters in a pressure profile that makes racetrack equilibria [Eq. (1) with $e = g = 0$], the computed equilibria can be made to match radial experimental data quite closely. It is found that the best match between theory and experiment occurs when $\beta_s \simeq 0.6$, suggesting that this is the value obtained in the experiments (this quantity is difficult to measure). These equilibria are, however, too racetracklike in shape to match the axial experimental data. To make equilibria that have elliptical separatrices and a gentle distribution of flux surfaces in the axial direction, it was found necessary to make $p(\psi)$ very steep as a function of ψ at the separatrix. There may be other ways to make the equilibria less racetracklike in shape, but we were unable to find any of them. Of course, the computations were made with the MHD model; it is possible that kinetic equilibria would match the experimental data more naturally.

ACKNOWLEDGMENTS

The authors acknowledge useful discussions with D. E. Shumaker and J. L. Schwarzmeier.

This work was performed under the auspices of the U.S. Department of Energy.

APPENDIX A: AVERAGE BETA CONDITION WITH END MIRRORS

Here we evaluate the contribution of the end mirrors to the average-beta condition. We consider an elongated FRC of half-length l in equilibrium inside the coil geometry of Fig. 1. (The effect of mirrors on $\langle\beta\rangle$ in a different geometry has been discussed by Suzuki and Hamada.[18]) We assume that the pressure on open field lines is negligible. Following the derivation of Ref. 1, we consider a control surface that includes $r = 0$, the coil, $z = 0$, and a value of z under the end mirror (about 96 cm) at which the field lines are approximately straight. From the axial and radial MHD equilibrium relations[1] we obtain

$$\langle\beta\rangle = 1 - \frac{x_s^2}{2} - \frac{(r_w^2/r_m^2 - 1)(1 - x_s^2)^2}{2x_s^2} + \frac{1}{r_s^2}\int_{r_m}^{r_w}\left(\frac{B_m}{B_0}\right)^2 r\, dr, \tag{A1}$$

where B_m is the magnetic field on the coil where $B_r \neq 0$, and where B_0 is the value of the magnetic field at $r = r_w$ and $z = 0$. For a straight cylindrical coil ($r_m = r_w$), Eq. (A1) reduces to the usual condition, $\langle\beta\rangle = 1 - x_s^2/2$. For cases where l is substantially smaller that z_m, a control surface inside the straight portion of the coil can be used to recover this condition. In such cases, the mirror region is unaffected by the FRC, and we may denote B_m by B_{mv} and use a new control surface bounded by the straight field line region between the FRC and the mirror and the straight field line region under the mirror. Applying the previous arguments to this region we obtain

$$\frac{1}{r_s^2}\int_{r_m}^{r_w}\left(\frac{B_{mv}}{B_0}\right)^2 r\, dr = \frac{(r_w^2/r_m^2 - 1)(1 - x_s^2)^2}{2x_s^2}. \tag{A2}$$

Equations (A1) and (A2) can be combined to give

$$\langle\beta\rangle = 1 - \frac{x_s^2}{2} + \frac{1}{r_s^2}\int_{r_m}^{r_w} \frac{B_m^2 - B_{mv}^2}{B_0^2} r\,dr. \tag{A3}$$

For cases with $l \leqslant z_m$, the FRC somewhat compresses the magnetic field around the end mirror so that $B_m > B_{mv}$, giving values of $\langle\beta\rangle$ greater than $1 - x_s^2/2$ in Eq. (A3).

To obtain quantitative information from Eq. (A3), we used a vacuum magnetic field solver[6] and the geometry of Fig. 1. The separatrix was modeled as a conductor of midplane radius $r_s = 10$ cm ($x_s = 0.4$) with an elliptical shape in the axial direction, i.e., $r_s(z) = r(0)(1 - z^2/l^2)^{1/2}$, where l is the separatrix length. The values of $\langle\beta\rangle$ so obtained from Eq. (A3) are shown in Fig. 6. For $l \leqslant 50$ cm, the contribution of the end mirror is negligible and $\langle\beta\rangle = 0.92$. For $l \geqslant 50$ cm, $\langle\beta\rangle$ increases with l. In particular, for $l \simeq z_m$, Eq. (A3) gives $\langle\beta\rangle \simeq 0.95$, in excellent agreement with the values obtained from the two-dimensional calculation for the case shown in Fig. 1. Another equilibrium with $l \simeq 70$ cm gave $\langle\beta\rangle = 0.93$, also in agreement with Eq. (A3). These computed values are given in Fig. 6 with solid circles. Furthermore, the values of $\langle\beta\rangle$ given in Fig. 6 are found to be insensitive to whether the mirror is formed by a smooth shape change of the coil, as in the computation, or by a sharp step at $z = z_m$, as in the experiment.

Finally, one should note that the increase in $\langle\beta\rangle$ due to the end mirrors decreases as the plasma radius increases. For example, for $l = 80$ cm, this increase is 3% for $x_s = 0.4$, 2.5% for $x_s = 0.5$, and 2% for $x_s = 0.6$, as found with the above described numerical procedure. Because $\langle\beta\rangle$ decreases as x_s increases, the pressure profile becomes more diffuse and the influence of the end mirrors rapidly becomes negligible. For example, substantial reductions in particle confinement time τ_N and magnetization $\bar{s}$ are shown in Table I for $x_s = 0.4$. For similar plasma parameters but $x_s = 0.6$, those reductions are less than 5%. This is favorable for future FRC experiments where larger values of x_s are desired.

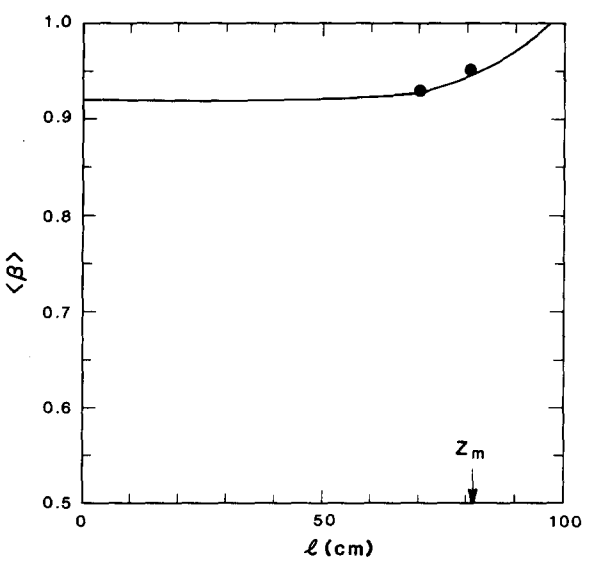

FIG. 6. The average β is displayed as a function of the plasma length l for the FRX-C coil geometry. The solid line is obtained from Eq. (A3); the solid circles are values from numerically computed equilibria.

APPENDIX B: THE EFFECT OF TOROIDAL FIELD

A question that is often asked about FRC's is whether they have some toroidal field in addition to the dominant poloidal field and, if so, how much. Some answers have been obtained recently in the translation experiments on FRX-CT where toroidal fields as large as $\frac{1}{3}$ of the field at the wall have been measured.[19] The effect of toroidal field will be discussed here within the limits of equilibrium theory.

The first thing to examine is the effect of toroidal field on the average beta for very long FRC's. In the midplane of such a FRC the radial equilibrium condition is

$$\frac{d}{dr}\left(p + \frac{1}{2\mu_0}(B_z^2 + B_\theta^2)\right) + \frac{B_\theta^2}{r} = 0, \tag{B1}$$

whereas the axial equilibrium condition is

$$\int_0^{r_s}\left(p + \frac{1}{2\mu_0}(B_\theta^2 - B_z^2)\right) r\,dr = \frac{B_0^2 r_s^2}{4\mu_0}(1 - x_s^2). \tag{B2}$$

(For simplicity it is assumed that there is no pressure outside of the separatrix.) Integrating Eq. (B1), substituting it into Eq. (B2), and integrating by parts yields the following condition for the average beta:

$$\langle\beta\rangle = 1 - \frac{1}{2}x_s^2 - \frac{1}{r_s^2}\int_0^{r_s}\left(\frac{B_\theta}{B_0}\right)^2 r\,dr. \tag{B3}$$

Hence, adding toroidal field always reduces the average beta, but not by very much. For instance, if the peak toroidal field were less than $\frac{1}{3}$ of the main field at the wall, as observed in recent experiments, then the correction to the average beta would typically be less than 5%. An effect this small would be quite difficult to detect experimentally in present experiments.

A natural question is whether toroidal field could be the cause of the gentle axial distribution of flux surfaces observed in the experiment. A rather simple argument can be made that it should not be by noting that all that happens when toroidal field is introduced is that the right-hand side of the Grad–Shafranov equation is modified somewhat. The equation is still elliptic, and the boundary conditions are still the same; it would seem that solutions of the same kind should be obtained if the right-hand side with toroidal field is

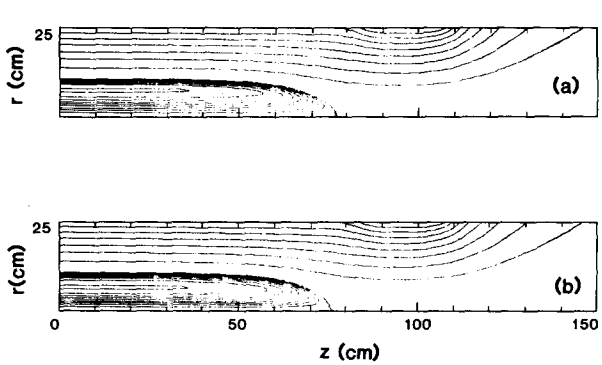

FIG. 7. Two equilibria are displayed here. Both have $x_s = 0.43$ and $\beta = 0.6$. Case (a) has no toroidal field while case (b) has a ratio of the peak toroidal field to the peak poloidal field of 0.47. The equilibrium parameters for (a) are $a1 = -38.9$, $b1 = 53.6$, $c = 97.6$, $e1 = 0.0$, $\eta = 0.0$. The equilibrium parameters for (b) are $a = -38.9$, $b = 53.6$, $c = 88.1$, $e = 0.0$, $\eta = 0.97$. In the computation there were 53 radial mesh points and 96 axial mesh points.

not radically different from the right-hand side without it. In particular, note that the toridal field term in the equilibrium equation must vanish at the separatrix, so the kind of peaking of the right-hand side that was found to produce less racetracklike equilibria cannot be supplied by the addition of toroidal field. To verify this rather loose argument, we computed FRC equilibria in the geometry of Fig. 1 including toroidal field. The equilibrium equation that was solved is

$$r\frac{\partial}{\partial r}\left(\frac{1}{r}\frac{\partial\psi}{\partial r}\right)+\frac{\partial^2\psi}{\partial z^2}=-r^2\frac{dp}{d\psi}-I\frac{dI}{d\psi}, \tag{B4}$$

where $\mathbf{B}=\nabla\psi\hat{\theta}/r+I(\psi)\hat{\theta}/r$. For simplicity, we chose $I(\psi)=c^{1/2}\eta\psi$ so that $I\,dI/d\psi=c\eta^2\psi$. The constant c is the same one that appears in Eq. 1; it is adjusted by the equilibrium code as it iterates. In Fig. 7 two equilibria are displayed: (a) has no toroidal field, while the other (b) has a ratio of the peak toroidal field to the peak poloidal field of 0.47. For (a), $\langle\beta\rangle=0.92$ while for (b), $\langle\beta\rangle=0.85$. Both values are a little higher than predicted by Eq. (B3) because of the end mirror, but the difference between them is precisely given by the toroidal field correction term. Note that there is almost no change in the axial distribution of the flux surfaces.

[1]W. T. Armstrong, R. K. Linford, J. Lipson, D. A. Platts, and E. G. Sherwood, Phys. Fluids **24**, 2068 (1981).
[2]R. L. Spencer and D. W. Hewett, Phys. Fluids **25**, 1365 (1982).
[3]D. W. Hewett and R. L. Spencer, Phys. Fluids **26**, 1299 (1983).
[4]M. Tuszewski, Plasma Phys. **26**, 991 (1984).
[5]K. F. McKenna, W. T. Armstrong, R. R. Bartsch, R. E. Chrien, J. C. Cochrane, Jr., R. W. Kewish, Jr., P. Klingner, R. K. Linford, D. J. Rej, E. G. Sherwood, R. E. Siemon, and M. Tuszewski, Phys. Rev. Lett. **50**, 1787 (1981).
[6]M. Tuszewski, Phys. Fluids **24**, 2126 (1981).
[7]D. J. Rej and W. T. Armstrong, Nucl. Fusion **24**, 177 (1984).
[8]M. Tuszewski, in *Proceedings of the Sherwood Theory Meeting in Arlington 1983* (University of Maryland, College Park, MD, 1983), Paper 1Q4.
[9]D. S. Harned, Phys. Fluids **26**, 1320 (1983).
[10]A. Eberhagen and W. Grossmann, Z. Phys. **248**, 130 (1971).
[11]M. Tuszewski and R. K. Linford, Phys. Fluids **25**, 765 (1982).
[12]J. T. Slough, A. L. Hoffman, R. D. Milroy, D. G. Harding, and L. C. Steinhauer, Nucl. Fusion **24**, 1537 (1984).
[13]M. Tuszewski and K. F. McKenna, Phys. Fluids **27**, 1058 (1984).
[14]J. L. Schwarzmeier, D. C. Barnes, D. W. Hewett, C. E. Seyler, A. I. Shestakov, and R. L. Spencer, Phys. Fluids **26**, 1295 (1983).
[15]D. E. Shumaker, J. Comp. Phys. **53**, 456 (1984).
[16]W. Grossmann and J. Saltzmann, in *Megagauss Physics and Technology* (Plenum, New York, 1980), p. 403.
[17]D. E. Shumaker, Bull. Am. Phys. Soc. **29**, 1327 (1984).
[18]K. Suzuki and S. Hamada, J. Phys. Soc. Jpn. **53**, 16 (1984).
[19]W. T. Armstrong and R. E. Chrien (private communication, 1984).